Journal of Membrane Science 599 (2020) 117840

Contents lists available at ScienceDirect

Journal of Membrane Science

journal homepage: http://www.elsevier.com/locate/memsci

Efficient and selective ethane-to-ethylene conversion assisted by a mixed proton and electron conducting membrane

Shichen Sun, Kevin Huang *

Department of Mechanical Engineering, University of South Carolina, USA

ARTICLE INFO

Keywords:
Membrane reactor
Mixed conductor
Conversion
Selectivity
Durability

ABSTRACT

Direct conversion of alkanes into valuable chemicals has attracted significant interest in recent decades by academia and industry alike due to the vast economic potential. One type of such conversions is non-oxidative dehydrogenation (NODH), which is deemed advantageous over its oxidative counterpart in conversion and selectivity. However, coking-related degradation is a major challenge to the NODH route. We here demonstrate an efficient and selective ethane-to-ethylene conversion membrane reactor operating on NODH and a mixed electron and proton conductor (MEPC) having a composition of $BaCo_{0.4}Fe_{0.4}Zr_{0.1}Y_{0.1}O_3$ (BCFZY). The H_2 produced from NODH is instantly removed by BCFZY, thus shifting the equilibrium to maximize conversion and selectivity. The results show that the single-pass ethane-to-ethylene conversion, ethylene selectivity and product yield at 700 °C are 70, 90 and 63%, respectively, with a moistened ethane as the feedstock. During a 100-h durability testing, there is virtually no degradation observed in membrane performance.

1. Introduction

Non-oxidative dehydrogenation of ethane (NODHE) to ethylene represents an attractive alternative to steam cracking (SC), the current benchmark technology for mass production of ethylene, because it promises high selectivity and conversion at reduced temperature range of 600–700 °C, thus lowering energy consumption and carbon emissions [1–5]. In theory, the NODHE process can be combined with a H_2-permeable membrane to shift the thermodynamic equilibrium toward ethylene production by extracting H_2 produced from the thermal dehydrogenation of ethane (TDHE). Unfortunately, the conventional Pd-based H_2 permeation membrane is not suited for NODHE application because it would not be stable in the temperature range of ethane dehydrogenation reaction (>600 °C to be thermodynamically favorable). Therefore, most of membrane based NODHE reactors demonstrated so far utilizes ceramic proton conducting membranes with electrical field as the driving force. For example, with an electrolysis cell using Pt as both cathode and anode, and $BaCe_{0.85}Y_{0.1}Nd_{0.05}O_{3-\delta}$ (BCYN) as electrolyte, Fu et al. reported a ~92.6% selectivity and ~35.5% conversion at 700 °C with a feed of pure C_2H_6 [6]. With a fuel cell configuration using a proton conducting electrolyte and $(Pr_{0.4}Sr_{0.6})_3(Fe_{0.85}Mo_{0.15})_2O_7$ (PSFM) infiltrated with Co–Fe alloy nanoparticles as anode, Liu et al. also reported a co-production of electricity and ethylene at 45.4% conversion, 91.4% selectivity and 41.5% yields at 750 °C [7].

In these oxide proton-conductor based electrolysis cells, it is generally believed that the ethane-to- ethylene conversion follows a sequential two-step chemical and electrochemical reactions at the anode:

$$\text{Thermal dehydrogenation reaction: } C_2H_6 = C_2H_4 + H_2 \quad (1)$$

$$\text{Electrochemical oxidation reaction: } H_2 + 2O_O^X = 2OH_O^{\cdot} + 2e^- \quad (2)$$

where the proton species $OH_O^{\cdot}$ is formed in oxides by dissolving H_2 and releasing electrons [8]. The protons are then transferred under a H_2-chemical-poetntial gradient by hopping through oxygen lattices (O_O^X) [9], until combining with electrons to release hydrogen at the cathode:

$$2OH_O^{\cdot} + 2e^- = 2O_O^X + H_2 \quad (3)$$

A common feature of ODHE electrolysis cells is the use of an external circuit to accept or provide electrons for the electrode reactions, which requires additional electrical components and subsystems. This would add cost and complexity to the overall system. To this end, use of mixed ionic and electronic conductors as the membrane for the above conversion offers a simplified option by eliminating external electrical circuit since electrons are provided by the membrane itself. Early studies on using mixed oxide-ion and electron conductors (MOECs) as oxygen

* Corresponding author.
E-mail addresses: sun68@mailbox.sc.edu (S. Sun), huang46@cec.sc.edu (K. Huang).

https://doi.org/10.1016/j.memsci.2020.117840
Received 19 December 2019; Received in revised form 3 January 2020; Accepted 11 January 2020
Available online 13 January 2020

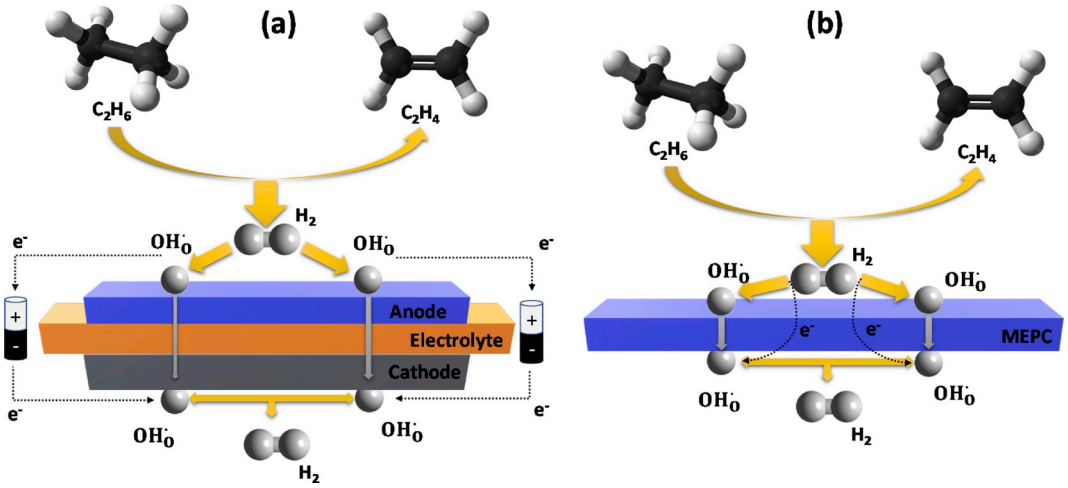

Fig. 1. Schematic of (a) proton conducting electrolysis cell and (b) MEPC membrane for dehydrogenation of ethane to ethylene.

transport membranes (OTMs) to separate oxygen from air have shown simplified design and cost saving at commercial scale [10–12]. Following the same principle, use of MEPCs to separate H_2 from a H_2-containing stream is also possible. Fig. 1 compares the working principle of a proton-conducting-electrolyte-based electrolysis cell and MEPC membrane reactor using ethane-to-ethylene conversion as an example for illustration purpose. The underlying chemical/electrochemical reactions at the two surfaces are expressed by the reaction (1)-(3), but with a distinction in the source of electrons. Due to its non-oxidative nature, over-oxidation of the more active product (e.g. ethylene) can be considerably mitigated, thus improving the product selectivity.

Use of MEPCs membrane reactors to upcycle methane [13,14], ethane [15] and propane [16,17] has been well-documented in the literature. However, one of the challenges for MEPCs-based membrane reactors is the poor long-term stability caused by coking and CO_2 attack [18–20]. To further advance the commercial development of MEPC-based membrane reactors, this stability issue must be overcome.

We here report the performance (conversion, selectivity and yield) of a MEPC-based membrane based on a perovskite structured oxide $BaCo_{0.4}Fe_{0.4}Zr_{0.1}Y_{0.1}O_{3-\delta}$ (BCFZY) in a reactor converting ethane into ethylene without catalyst and electricity. Note that we select a single-phase composition such as BCFZY over other two-phase counterparts such as BCFZY + Ni for the consideration of maximizing mixed ion/electron transport and thus flux. On the other hand, to mitigate coking as well as providing a favorable working condition for the BCFZY (enhancing proton conductivity with steam) [8], we use moistened ethane and Ar as the feed and sweep gas, respectively, for the study.

2. Experimental procedure

2.1. Synthesis and fabrication of the MEPC membrane

The composition of the MEPC used in this study is $BaCo_{0.4}Fe_{0.4}Zr_{0.1}Y_{0.1}O_{3-\delta}$ (denoted as BCFZY). It was synthesized via a glycine nitrate process (GNP). Briefly, stoichiometric amounts of precursors including $Ba(NO_3)_2$ (#10180117, Alfa Aesar, 99%), $Co(NO_3)_2{\cdot}6H_2O$ (#239267, Alfa Aesar, 99%), $Fe(NO_3)_3{\cdot}9H_2O$ (#216828, Alfa Aesar, 99%), $ZrO(NO_3)_2{\cdot}xH_2O$ (#43224, Alfa Aesar, 99.9%), $Y(NO_3)_3{\cdot}6H_2O$ (#12898, Alfa Aesar, 99.9%) were first dissolved in distilled water. Glycine was then added to the solution with the molar ratio of 1:1 (glycine to total metal ions). The solution was then heated on a hotplate until boiling and self-combustion. The powders were finally collected and further calcined at 1000 °C for 2 h in air. The as-synthesized BCFZY powder was examined by X-Ray diffraction (Rigaku 2005H302) for phase identification.

Dense BCFZY membrane discs (φ20 mm × 0.8 mm thickness) were made by dry pressing the above powder at 200 MPa and sintering at 1275 °C for 5 h. The microstructures of both surface and cross-section of the sintered membranes were examined with a field emission scanning electron microscope (Zeiss Ultra plus FESEM).

2.2. Ethane conversion test

Ethane conversion tests were carried out on the BCFZY membrane using a homemade permeation reactor system. First, a BCFZY dense membrane was sealed onto a supporting alumina tube using silver paste. A second short alumina tube was then bonded onto the top of the membrane to guide the feed gas. The assembly was first cured at 150 °C for 2 h prior to ramping up to higher temperatures. At the testing temperature, a humidified C_2H_6–Ar was fed to one side (denoted as feed side) of the BCFZY membrane at a flow of 100 mL/min as the feed gas. The compositions (C_2H_6, C_2H_4, CH_4, CO, CO_2, H_2) of the C_2H_6 stream effluent was constantly analyzed by an online gas chromatography (GC) (Agilent 490). In the meanwhile, the other side (denoted as sweep side) of the BCFZY membrane was swept by a 3%-humidified Ar with a flow rate of 50 mL/min. The compositions of the effluent from the sweep (Ar) side is simultaneously analyzed with another GC. The effect of reactor temperature on conversion was tested from 650 to 750 °C in a step of 50 °C; at each temperature there is a 1-h hold time before GC sampling. To make a comparison with moistened ethane conversion, a dry 2.5% C_2H_6–Ar at 100 mL/min was also used as the feed gas, while a dry Ar at 50 mL/min is used as the sweep gas. The effective thickness and surface area of the membrane is 0.8 mm and 0.95 cm^2, respectively.

The effect of C_2H_6 concentration on conversion performance was tested with two ranges of C_2H_6 concentrations; at low concentration range, i.e. 1.25, 2.5 and 3.75%, the test was carried out with 3%-humidified feed gas; while at elevated C_2H_6 concentrations, i.e. 5, 10, 15, 20 and 25%, the test used a higher 12% steam to minimize coking during test. The reactor temperature was fixed at 700 °C. On the other hand, the effect of H_2O concentration on conversion performance was also studied at 700 °C. In this case, a dry 25%C_2H_6/Ar was humidified with 3, 6 and 12% of steam as the feed gas; different steam contents were generated by passing dry 25%C_2H_6/Ar through a bubbler at different temperatures. Last, long-term stability of the membrane reactor is evaluated at 700 °C for ~100 h using a 3%-humidified 1.25%C_2H_6/Ar as the feed gas. During the above tests, the total flow rate of the feed gas was fixed to 100 mL/min.

In addition, to confirm the effectiveness of MPEC membrane in promoting ethane dehydrogenation performance, a blank experiment

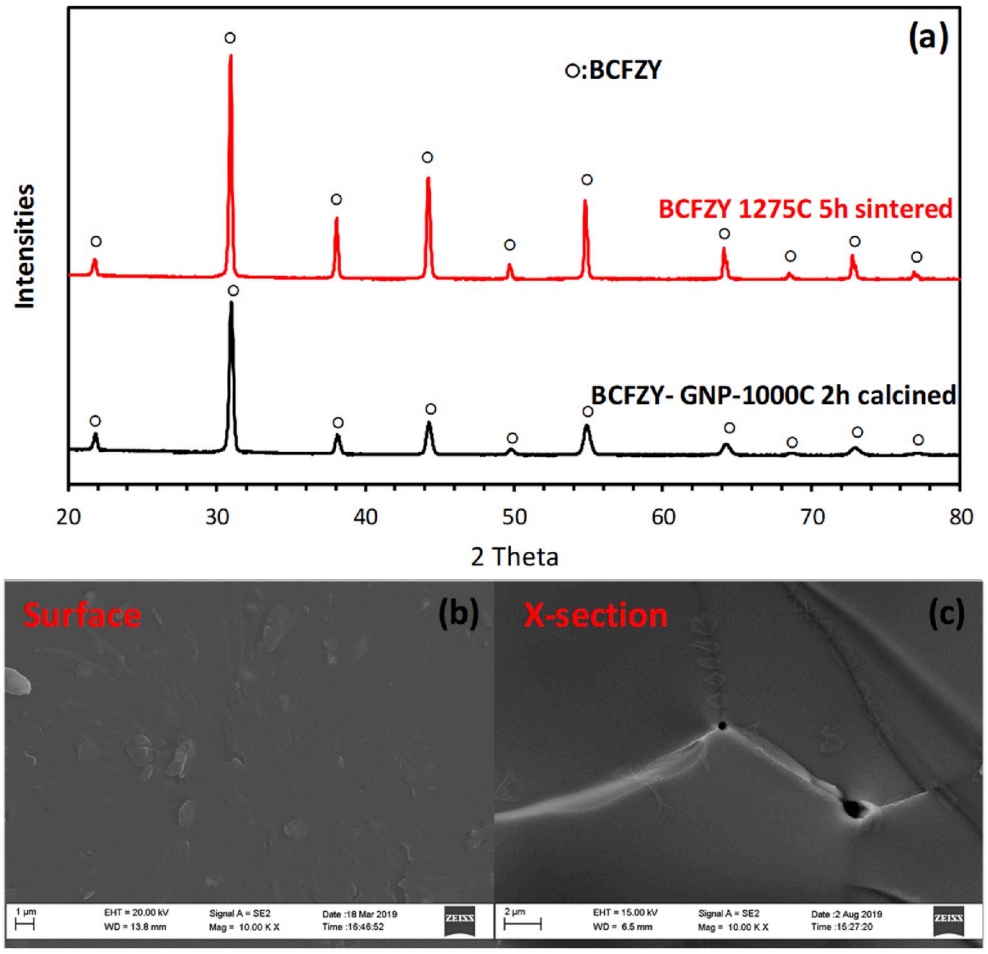

Fig. 2. (a) XRD pattern of GNP-synthesized BCFZY powder after 1000 °C for 2 h and 1275 °C for 5 h, and SEM images of (b) surface and (c) cross-section of BCFZY membrane sintered at 1275 °C for 5 h.

with a dense Al_2O_3 disk was also carried out at 700 °C with a 3%-humidified feed gas containing 1.25-3.75% ethane.

From the measured concentrations, flux densities of CH_4, CO_2, CO, C_2H_4 and H_2, denoted by J_{CH4}, J_{CO2}, J_{CO}, J_{C2H4}, and J_{H2}, respectively, on the C_2H_6 side (feed side), are calculated by:

$$J_{CH_4} = \frac{C_{CH_4}}{1 - C_{CH_4} - C_{CO_2} - C_{CO} - C_{C_2H_6} - C_{C_2H_4} - C_{H_2}(\text{feed})} \times \frac{F_{Ar}^f}{A} \quad (4)$$

$$J_{CO_2} = \frac{C_{CO_2}}{1 - C_{CH_4} - C_{CO_2} - C_{CO} - C_{C_2H_6} - C_{C_2H_4} - C_{H_2}(\text{feed})} \times \frac{F_{Ar}^f}{A} \quad (5)$$

$$J_{CO} = \frac{C_{CO}}{1 - C_{CH_4} - C_{CO_2} - C_{CO} - C_{C_2H_6} - C_{C_2H_4} - C_{H_2}(\text{feed})} \times \frac{F_{Ar}^f}{A} \quad (6)$$

$$J_{C_2H_4} = \frac{C_{C_2H_4}}{1 - C_{CH_4} - C_{CO_2} - C_{CO} - C_{C_2H_6} - C_{C_2H_4} - C_{H_2}(\text{feed})} \times \frac{F_{Ar}^f}{A} \quad (7)$$

$$J_{C_2H_6} = \frac{C_{C_2H_6}}{1 - C_{CH_4} - C_{CO_2} - C_{CO} - C_{C_2H_6} - C_{C_2H_4} - C_{H_2}(\text{feed})} \times \frac{F_{Ar}^f}{A} \quad (8)$$

$$J_{H_2} = \frac{C_{H_2}}{1 - C_{CH_4} - C_{CO_2} - C_{CO} - C_{C_2H_6} - C_{C_2H_4} - C_{H_2}(\text{feed})} \times \frac{F_{Ar}^f}{A} \quad (9)$$

where F_{Ar}^f is the flow rate of the Ar in the feed gas, i.e. (1-x) × 100 mL/min (x is the concentration of C_2H_6; 100 mL/min is the total flow); and A is the effective area of the sample.

Similarly, H_2 flux density produced at the sweep side is calculated by

$$J_{H_2}(\text{sweep}) = \frac{C_{H_2}(sweep)}{1 - C_{H_2}(sweep)} \times \frac{F_{Ar}^s}{A} \quad (10)$$

where F_{Ar}^s is the flow rate of the sweeping Ar, i.e. 50 mL/min.

The ethane conversion ($X_{C_2H_6}$), C_2H_4 selectivity ($S_{C_2H_4}$), selectivity yield ($Y_{C_2H_4}$), coking rate (R_C) and H_2 recovery rate are calculated by:

$$X_{C_2H_6} = \frac{F_{C_2H_6(in)} - F_{C_2H_6(out)}}{F_{C_2H_6(in)}} \times 100\% \quad (11)$$

$$S_{C_2H_4} = \frac{J_{C_2H_4} \times A}{F_{C_2H_6(in)} - F_{C_2H_6(out)}} \times 100\% \quad (12)$$

$$Y_{C_2H_4} = S_{C_2H_4} \times X_{C_2H_6} \quad (13)$$

$$R_C = [2F_{C_2H_6} - (J_{CO_2} + J_{CO} + J_{CH_4} + 2J_{C_2H_4} + 2J_{C_2H_6}) \times A] / 22.4 \times 10^{-3} \quad (14)$$

$$R_{H_2} = \frac{J_{H_2}(sweep)}{J_{H_2}(feed)} \times 100\% \quad (15)$$

2.2.1. Post conversion analysis

All membranes subject to conversion testing were characterized by XRD for any secondary phase formation and SEM/EDS for microstructural and chemical changes.

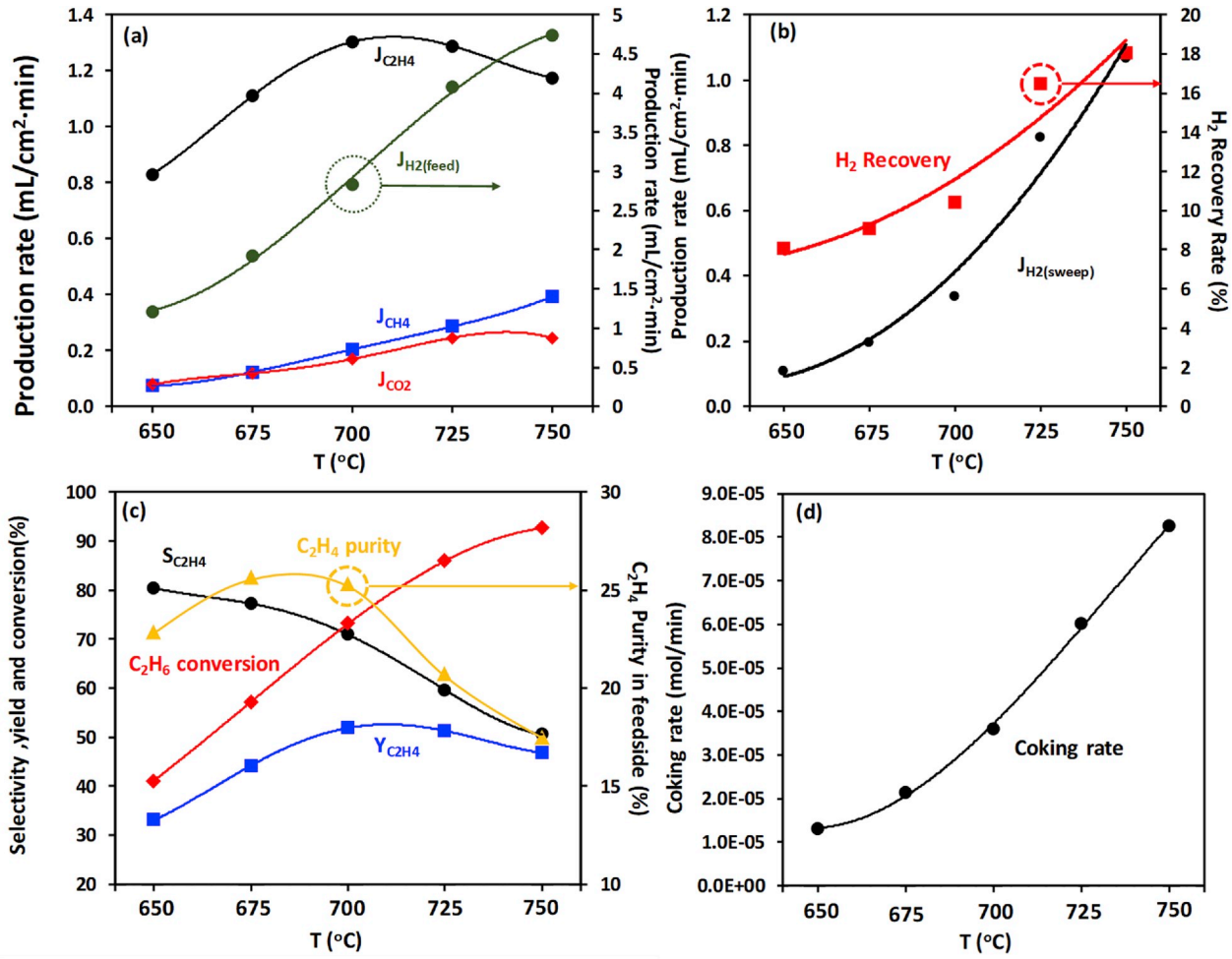

Fig. 3. (a) Production rate of C_2H_4, CH_4, CO_2 and H_2 in the effluent stream of the feed side; (b) production rate of H_2 in the effluent stream of the sweep side (Ar); (c) conversion rate of C_2H_6 and selectivity and yield of C_2H_4; and (d) coking rate vs temperature.

3. Results and discussion

3.1. Phase purity and microstructure of the membrane

The XRD pattern of the synthesized BCFZY powder is shown in Fig. 2 (a), where a pure primitive cubic perovskite phase is formed at 1000 °C for 2 h and maintained after sintering at 1275 °C for 5 h [20]. The surface and cross-sectional microstructures of the sintered BCFZY are shown in Fig. 2 (b) and (c), where a dense surface and bulk with a very few of closed micro-size pores are visible after sintering the membrane at 1275 °C for 5 h.

3.2. Moistened and un-moistened ethane conversion

With 3%H_2O-97%(2.5%C_2H_6–Ar) as the feed gas, the NODHE membrane performance was evaluated, and the results are shown in Fig. 3. The main products from the feed side are C_2H_4, H_2 with minor amount of CH_4, CO_2 and unreacted C_2H_6, but no CO was found. It is also worth mentioning that the concentrations of C_2H_4, CH_4 and CO_2 are all less than <0.01% at the sweep side (Ar) of the membrane, suggesting a good gas tightness of the membrane and adequate sealing. The measured gas compositions suggest some side reactions other than main reaction (1) concurrently take place during the conversion. These possible side reactions are:

Coking reaction: $C_2H_6 = C + CH_4 + H_2$ (16)

Coking reaction: $C_2H_6 = 2C + 3H_2$ (17)

Hydrolysis reaction: $C_2H_6 + H_2 = 2CH_4$ (18)

Decoking reaction: $C + 2H_2O = CO_2 + 2H_2$ (19)

Since C_2H_4 concentration is much higher than CH_4 and CO_2, the major reaction is still reaction (1). However, reactions (14–16) are not negligible, depending on how fast H_2 is extracted by the membrane. Reaction (17) is a de-coking reaction, the effectiveness of which determines the degree of coking and critically the lifespan of the reactor.

The production rate of C_2H_4 shown in Fig. 3(a) increases with temperature, i.e. from 0.82 to 1.34 mL/cm^{2}min from 650 to 700 °C, respectively, but slightly decreases after 700 °C, implying that 700 °C might be the optimal operating temperature for the membrane. On the other hand, the production rates of CH_4 and H_2 all increase with temperature from 650 to 750 °C, while CO_2 production rate also increases with temperature until reaching a plateau at 750 °C. At the same time, Fig. 3(b) shows a pure stream of H_2 at the sweep side with its flux increasing with temperature, but at a lower magnitude compared to the feed side. A possible reason for the low H_2 flux permeated is the thick membrane used in the study. With thin-film membrane configuration, the H_2 removal from the feed side is expected to be more effective.

Fig. 3(c) shows that the selectivity of C_2H_4 decreases from 81% at 650 °C to 51% at 750 °C, while the C_2H_6 conversion rate increases monotonously from 42% at 650 °C to 92% at 750 °C. At 700 °C, the yield is ~52%, which is comparable to steam cracking [21]; but the latter's operating temperature is 900 °C. The opposite trend in selectivity and

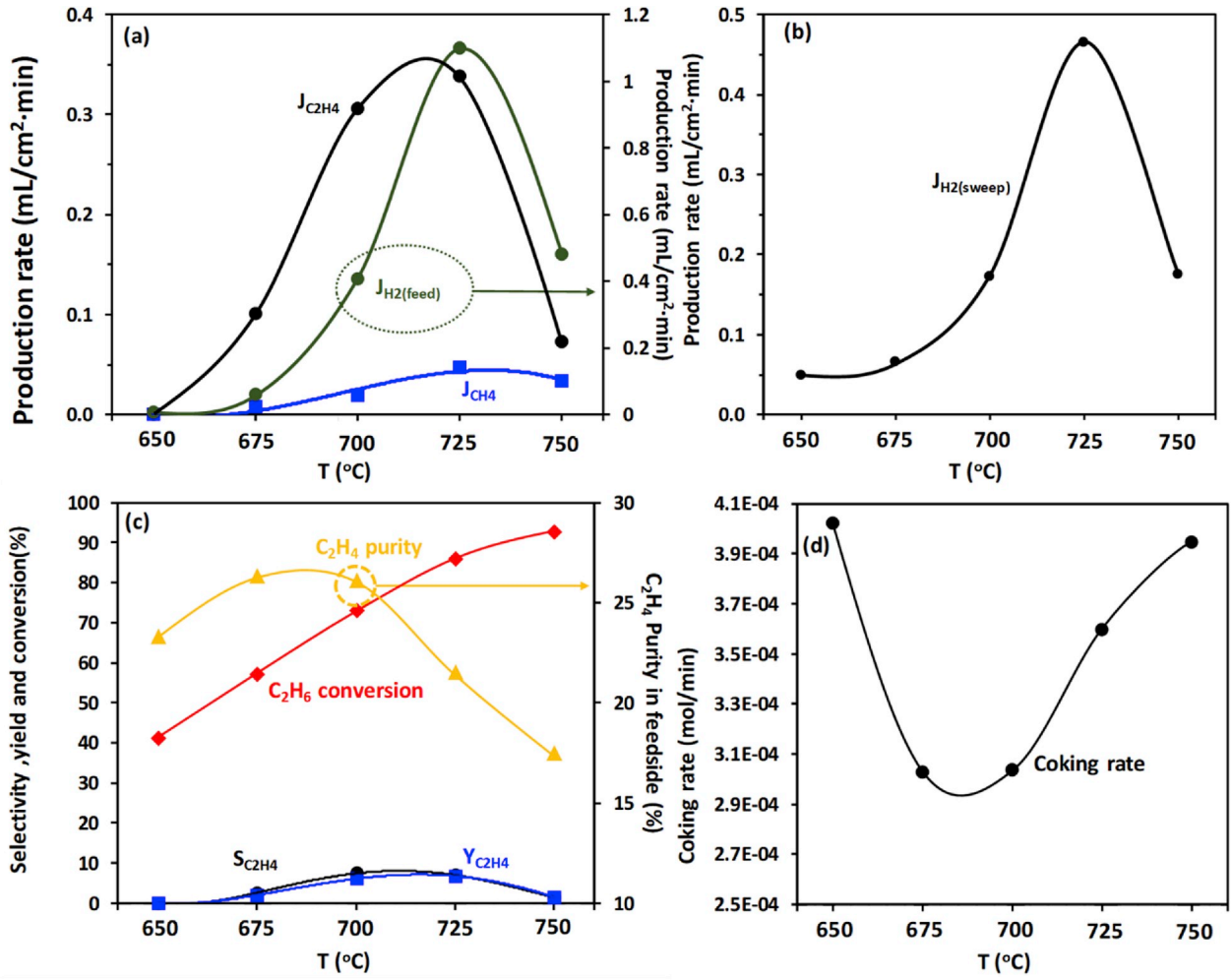

Fig. 4. (a) Production rates of C_2H_4, CH_4 and H_2 in the effluent at the feed side; (b) production rate of H_2 in the effluent at the sweep side (Ar); (c) C_2H_6 conversion and selectivity, yield and purity of C_2H_4; and (d) coking rate under dry condition.

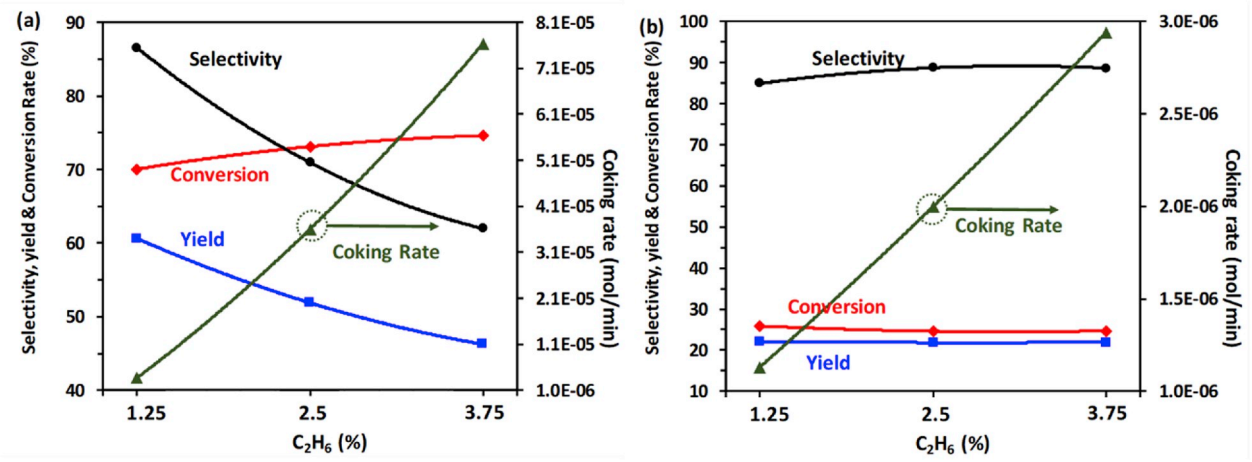

Fig. 5. C_2H_6 conversion and selectivity and C_2H_4 yield, and coking rate in (a) BCFZY membrane and (b) Al_2O_3 dense disk with 3% moistened 1.25, 2.50 and 3.75% of C_2H_6 as the feed gas at 700 °C.

conversion has resulted in a peak yield at 700 °C. The net results of the main reaction (1) competing with side reactions (14)-(15) are the fundamental reasons for the observed conversion performance. From the carbon balance, the coking rate was also estimated and shown in Fig. 3(d). While there is roughly eight-fold swing in the coking rate from 650 to 750 °C, the absolute magnitude of the coking rate is generally low.

For comparison, NODHE performance under dry condition was also measured and the results are shown in Fig. 4. Lower flux density, selectivity and yield of C_2H_4 are clearly observed; especially at 650 °C

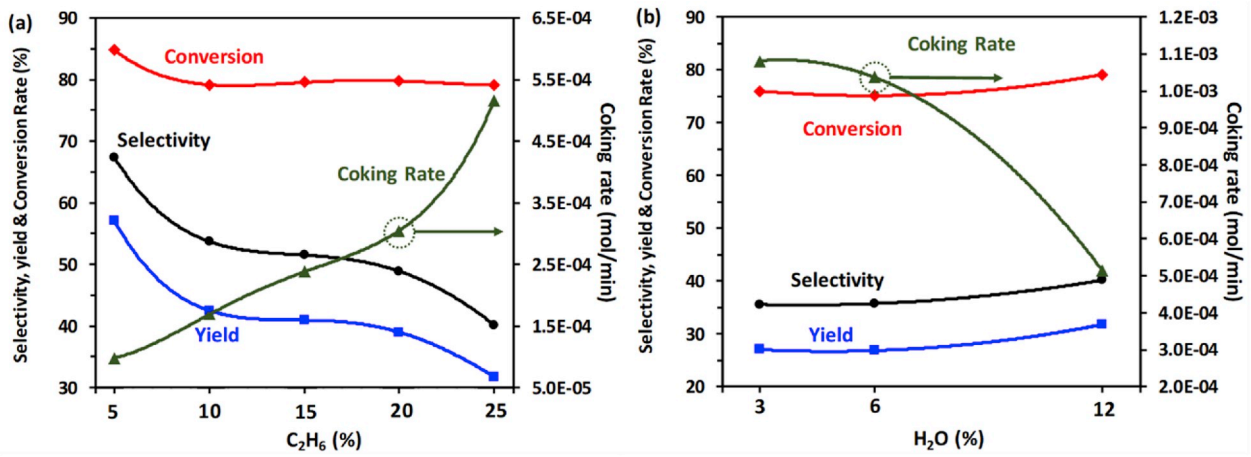

Fig. 6. C_2H_6 conversion and selectivity, C_2H_4 yield, and coking rate in the membrane reactor with (a) 12% humidified 5, 10, 15, 20 and 25% C_2H_6 and (b) 25% C_2H_6 humidified with 3, 6, and 12% H_2O at 700 °C.

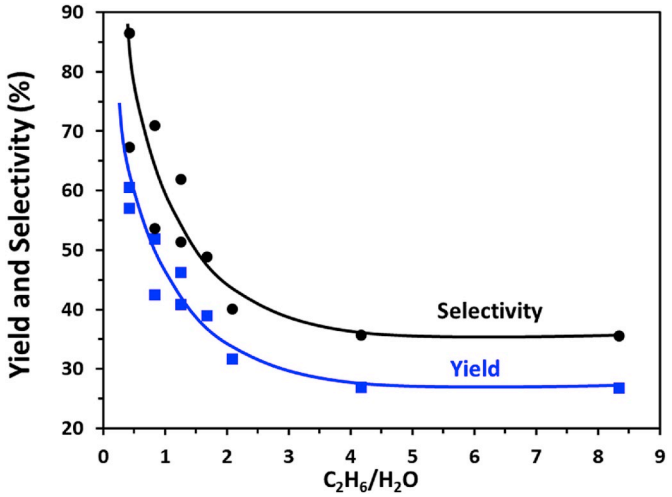

Fig. 7. Yield and selectivity for the BCFZY membrane with various C_2H_6/H_2O ratio at 700 °C.

there is almost no C_2H_4 in the product. In addition, CH_4 and H_2 production rates are also low and do not increase with temperature above 725 °C, while the conversion rate of C_2H_6 does increase with temperature, but it is mainly converted to coke. These observations suggest that a significant portion of ethane conversion in the reactor is likely through the coking reaction (14) and (15), covering the membrane with carbon and resulting in strange trends observed for fluxes of C_2H_4, CH_4, H_2 and coking rate shown in Fig. 4.

3.3. Effect of C_2H_6 and H_2O concentrations on ethane conversion and short-term stability

The effect of C_2H_6 concentration on ethane conversion performance at a relatively low range of 1.25-3.75% was examined at 700 °C and the results are shown in Fig. 5. As the C_2H_6 concentration increases from 1.25 to 3.75%, the selectivity and yield of C_2H_4 decrease from 87% and 61%–62% and 46%, respectively, while the C_2H_6 conversion slightly increases from 70% to 74%. On the other hand, the coking rate increases from 3.7×10^{-6} to 7.6×10^{-5} with the C_2H_6 concentration, indicating that higher C_2H_6 conversion at higher C_2H_6 concentrations is due to coking.

The blank experiment with a dense Al_2O_3 disk is more revealing. Fig. 5(b) shows a much lower conversion rate and yield (~25% and ~22%) with Al_2O_3 dense disk than the BCFZY membrane under the same conditions. These observations suggest that the BCFZY membrane does promote the ethane dehydrogenation by H_2 removal via the proton conducting membrane. However, the higher selectivity observed under these conditions suggests that the MPEC membrane may also remove H_2 resulted from side reactions such as reactions (16) and (17).

At high C_2H_6 concentrations, i.e. 5 to 25%, ethane conversion was evaluated with 12% humidification at 700 °C. Fig. 6 (a) shows that the selectivity and yield of C_2H_4 decrease from ~68% and ~57%–~40% and ~32%, respectively, while the C_2H_6 conversion slightly decreases from ~85 to ~79% as the C_2H_6 concentration increases. The most significant change with increasing C_2H_6 is the coking rate, with a dramatic increase from 9.8×10^{-5} to 5.2×10^{-4}.

For the H_2O concentration effect, a slight increase in both selectivity and yield is observed in Fig. 6(b) with increasing H_2O content from 3 to 12%, while there is no significant change in conversion. Moreover, coking rate is suppressed by increasing H_2O concentration, decreasing from 1×10^{-3} to 5×10^{-4}, suggesting that high steam concentration is needed for operating at high C_2H_6.

Based on above results, yield and selectivity of ethylene at 700 °C are plotted against C_2H_6/H_2O ratio and are shown in Fig. 7. An exponentially decreasing trend for both selectivity and yield are observed with C_2H_6/H_2O ratio, suggesting low C_2H_6/H_2O ratio is preferred for achieving better performance. Moreover, a plateau is reached as the ratio increases beyond certain point ($C_2H_6/H_2O \geq 2$, C_2H_6=25%, H_2O=3–12%), which may be attributed to the severe coking effect at 25% C_2H_6. Under this circumstance, ethane was mainly converted to carbon covering the membrane, making it insensitive to H_2O concentration change. The other reason may be the relatively small reactor area (~0.95 cm^2) used in this study that limits the dehydrogenation under high ethane concentration conditions.

A short-term stability test of 100 h was carried out at 700 °C using a 3% humidified 1.25% C_2H_6/Ar as feed gas. The results shown in Fig. 8 indicate no visible degradation in performance during operation. After cooling down to room temperature and disassembling the cell, no visible coking was observed on the membrane. This preliminary result suggests that membrane is chemically stable, and coking is suppressed under the relevant operating conditions.

3.4. Post-test analyses

To understand the surprising stability, post-test analysis was performed using XRD and SEM/EDS. Fig. 9 shows the XRD patterns, which indicate only a minor secondary phase of $BaCO_3$ among the original perovskite phase of BCFZY. In comparison, a significant amount of

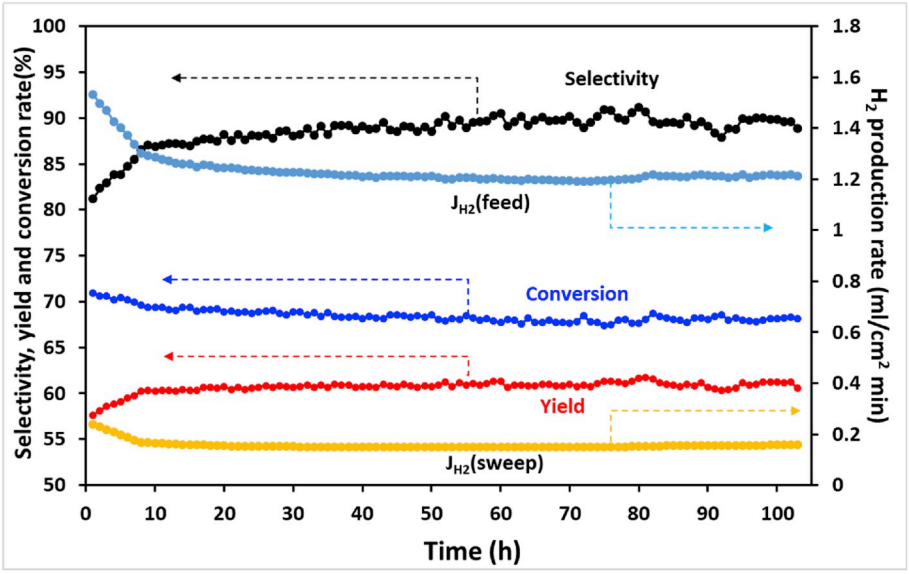

Fig. 8. Time-dependent conversion of C_2H_6, selectivity and yield of C_2H_4, and flux densities of H_2 on both sides of the membrane. Feed side: 3% humidified 1.25% C_2H_6/Ar; sweep side: Ar. Temperature: 700 °C.

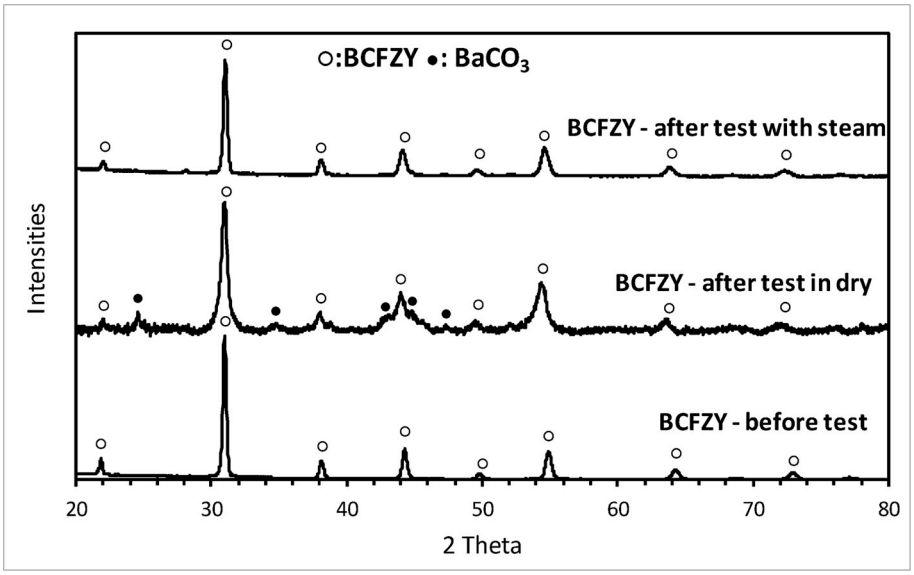

Fig. 9. XRD patterns of BCFZY membrane after testing in 3% humidified and dry ethane.

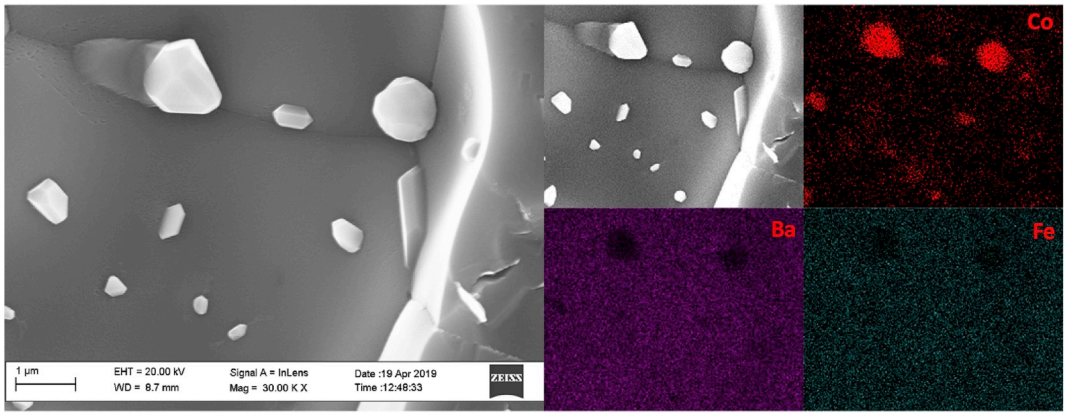

Fig. 10. SEM images and distributions of Co, Ba and Fe on the cross-section of BCFZY membrane after the test in 3%humidified feed gas.

$BaCO_3$ is detected on the BCFZY membrane after testing in dry C_2H_6. This observation suggests that the formation of $BaCO_3$ can be suppressed by steam. Similar phenomenon was also observed in similar materials such as BSCF [18], and BZCYYb [19].

The SEM/EDS analysis results of the tested BCFZY membrane are shown in Fig. 10. Nano-sized particles are clearly observed in the cross-sectional view. The EDS mapping suggests that these nano-sized particles contain pure cobalt. Given the fact that Co in BCFZY is reducible under the operating condition, this is a reasonable finding. In fact, these nano-sized cobalt particles could possibly serve as a catalyst for ethane dehydrogenation and may have certain contribution to the performance by providing additional electronic conductivity [3,4,22].

4. Conclusions

In summary, a simple but effective dehydrogenation of ethane to ethylene has been demonstrated using a MPEC membrane. With a 3% H_2O-moistened 1.25%C_2H_6–Ar as the feedstock, ~70% ethane conversion and 90% ethylene selectivity have been achieved at 700 °C with a minimal coking. From the effect of C_2H_6 and H_2O concentrations on conversion performance, a low C_2H_6/H_2O ratio is preferred to achieve a better conversion performance at 700 °C for a small lab-scale reactor. The BCFZY membrane also shows a good chemical and structural stability under the operating condition with the presence of steam. The exsolved Co nanoparticles may provide additional catalytic activity to the dehydrogenation reaction and electronic conductivity to the membrane.

Declaration of competing interest

The authors declare no conflicts of interest.

CRediT authorship contribution statement

Shichen Sun: Writing - original draft. **Kevin Huang:** Conceptualization, Supervision.

Acknowledgement

We would like to thank US Department of Energy, Office of Fossil Energy, National Energy Technology Laboratory (Award # DE-FE-0031634) and National Science Foundation (Award # CBET-1924095) for supporting this work.

References

[1] F. Cavani, N. Ballarini, A. Cericola, Oxidative dehydrogenation of ethane and propane: how far from commercial implementation? Catal. Today 127 (2007) 113–131.
[2] C.A. Gärtner, A.C. van Veen, J.A. Lercher, Oxidative dehydrogenation of ethane: common principles and mechanistic aspects, ChemCatChem 5 (2013) 3196–3217.
[3] Y. Schuurman, V. Ducarme, T. Chen, W. Li, C. Mirodatos, G. Martin, Low temperature oxidative dehydrogenation of ethane over catalysts based on group VIII metals, Appl. Catal. Gen. 163 (1997) 227–235.
[4] J. Sinfelt, W. Taylor, D. Yates, Catalysis over supported metals. III. Comparison of metals of known surface area for ethane hydrogenolysis, J. Phys. Chem. 69 (1965) 95–101.
[5] E. Thorsteinson, T. Wilson, F. Young, P. Kasai, The oxidative dehydrogenation of ethane over catalysts containing mixed oxides of molybdenum and vanadium, J. Catal. 52 (1978) 116–132.
[6] X.-Z. Fu, J.-L. Luo, A.R. Sanger, N. Danilovic, K.T. Chuang, An integral proton conducting SOFC for simultaneous production of ethylene and power from ethane, Chem. Commun. 46 (2010) 2052–2054.
[7] S. Liu, K.T. Chuang, J.-L. Luo, Double-layered perovskite anode with in situ exsolution of a Co–Fe alloy to cogenerate ethylene and electricity in a proton-conducting ethane fuel cell, ACS Catal. 6 (2015) 760–768.
[8] T. Norby, Ceramic proton and mixed proton-electron conductors in membranes for energy conversion applications, J. Chem. Eng. Jpn. 40 (13) (2007) 1166–1171.
[9] K.D. Kreuer, Proton-conducting oxides, Annu. Rev. Mater. Res. 33 (2003) 333–359.
[10] S. Hashim, A. Mohamed, S. Bhatia, Oxygen separation from air using ceramic-based membrane technology for sustainable fuel production and power generation, Renew. Sustain. Energy Rev. 15 (2011) 1284–1293.
[11] P.-M. Geffroy, J. Fouletier, N. Richet, T. Chartier, Rational selection of MIEC materials in energy production processes, Chem. Eng. Sci. 87 (2013) 408–433.
[12] J. Sunarso, S. Baumann, J. Serra, W. Meulenberg, S. Liu, Y. Lin, J.D. Da Costa, Mixed ionic–electronic conducting (MIEC) ceramic-based membranes for oxygen separation, J. Membr. Sci. 320 (2008) 13–41.
[13] G. Marnellos, O. Sanopoulou, A. Rizou, M. Stoukides, The use of proton conducting solid electrolytes for improved performance of hydro-and dehydrogenation reactors, Solid State Ion. 97 (1997) 375–383.
[14] S. Hamakawa, T. Hibino, H. Iwahara, Electrochemical hydrogen permeation in a proton-hole mixed conductor and its application to a membrane reactor, J. Electrochem. Soc. 141 (1994) 1720–1725.
[15] H. Iwahara, H. Uchida, S. Tanaka, High temperature-type proton conductive solid oxide fuel cells using various fuels, J. Appl. Electrochem. 16 (1986) 663–668.
[16] G. Karagiannakis, S. Zisekas, C. Kokkofitis, M. Stoukides, Effect of H2O presence on the propane decomposition reaction over Pd in a proton conducting membrane reactor, Appl. Catal. Gen. 301 (2006) 265–271.
[17] G. Karagiannakis, C. Kokkofitis, S. Zisekas, M. Stoukides, Catalytic and electrocatalytic production of H2 from propane decomposition over Pt and Pd in a proton-conducting membrane-reactor, Catal. Today 104 (2005) 219–224.
[18] S. Sun, Z. Cheng, Effects of H_2O and CO_2 on electrochemical behaviors of BSCF cathode for proton conducting IT-SOFC, J. Electrochem. Soc. 164 (2017) F88.
[19] L. Yang, S. Wang, K. Blinn, M. Liu, Z. Liu, Z. Cheng, Enhanced sulfur and coking tolerance of a mixed ion conductor for SOFCs: BaZr(0.1)Ce(0.7)Y(0.2-x)Yb(x)O(3-delta), Science 326 (2009) 126–129.
[20] C. Duan, R.J. Kee, H. Zhu, C. Karakaya, Y. Chen, S. Ricote, A. Jarry, E.J. Crumlin, D. Hook, R. Braun, Highly durable, coking and sulfur tolerant, fuel-flexible protonic ceramic fuel cells, Nature 557 (2018) 217.
[21] A. Pintér, A. Tungler, L. Nagy, L. Vida, L. Sebestyén, T. Gál, J. Kohán, J. Kerezsi, Comparative laboratory steam-cracking of different raw materials, React. Kinet. Catal. Lett. 88 (2006) 175–181.
[22] Y. Brik, M. Kacimi, M. Ziyad, F. Bozon-Verduraz, Titania-supported cobalt and cobalt–phosphorus catalysts: characterization and performances in ethane oxidative dehydrogenation, J. Catal. 202 (2001) 118–128.